Heteroatom-Doped Nickel Sulfide for Efficient Electrochemical Oxygen Evolution Reaction

Xingqun Zheng [1,2], Ling Zhang [2], Wei He [3], Li Li [2,*] and Shun Lu [4,5,*]

[1] College of Safety Engineering, Chongqing University of Science & Technology, Chongqing 401331, China

[2] State Key Laboratory of Power Transmission Equipment & System Security and New Technology, College of Chemistry and Chemical Engineering, Chongqing Univerisity, Chongqing 400044, China

[3] Department of Electrical Engineering and Computer Science, South Dakota State University, Brookings, SD 57007, USA

[4] Department of Agricultural Engineering, South Dakota State University, Brookings, SD 57007, USA

[5] Chongqing Institute of Green and Intelligent Technology, Chinese Academy of Sciences, Chongqing 400714, China

* Correspondence: liliracial@cqu.edu.cn (L.L.); shun.lu@sdstate.edu (S.L.)

Content info

1. Materials Synthesis

1.1 Materials

Nickel foam was purchased from Kunshan Kuangxun Ltd. (China). Pt/C (40% Pt on Vulcan XC-72R) and RuO_2 were purchased from Sigma-Aldrich Chemical Reagent Co., Ltd., and nickel nitrate hexahydrate ($Ni(NO_3)_2 \cdot 6H_2O$, 98.0%), ammonium fluoride (NH_4F, 98.0 %), Sublimed sulfur (S, 99.5%), Sodium hypophosphite monohydrate ($NaH_2PO_2 \cdot H_2O$, 85%) were bought from Shanghai Titan Science &

Technology Co., Ltd. The ultrapure water (>18 MΩ) was prepared from a Millipore system. All reagents were used as received without any purification.

1.2 Synthesis of Ni(OH)$_2$ NSs

The nickel hydroxide nanosheets were grown on nickel foam by a hydrothermal method. 1.4 mmol Ni(NO$_3$)$_2$·6H$_2$O, 2.8 mmol NH$_4$F and 7 mmol urea were dissolved in 35ml deionized water under vigorous stirring for 30 min. And then, The solution was then transferred into a 50 ml PTFE-lined stainless steel autoclave containing a piece of clean nickel foam (1×4 cm^2). The autoclave was sealed and heated at 150 °C for 6 h. Afterwards, the autoclave was cooled to room temperature and then its content was taken out and washed with ethanol and water in turn before being dried at 60°C in air for 12 h (denoted as Ni(OH)$_2$ NSs).

1.3 Synthesis Ni$_3$S$_2$ nanosheets and C doped Ni$_3$S$_2$ nanosheets

Sulfuration of the obtained Ni(OH)$_2$ NSs was accomplished in a horizontal quartz tube furnace. Specifically, Ni(OH)$_2$ nanosheets (NSs) and sublimed sulfur powder were put individually in two porcelain boats. The boat with sublimed sulfur powder was placed at the upstream end of the furnace and the boat with Ni(OH)$_2$ NSs at the other end. The molar ratio of metal to sublimed sulfur powder was 1:10. The furnace was heated to 350°C at a heating rate of 5°C min^{-1} and maintained for 2h in H$_2$/N$_2$ (v/v, 15/85) reduction atmosphere (55 sccm). Then the reaction system was cooled naturally down to room temperature in the furnace to obtain Ni$_3$S$_2$ NSs. Further, the as prepared Ni$_3$S$_2$ NSs was annealed at 400°C in CH$_4$/N$_2$ (v/v 1:1) for 2 h, and then the reaction system was cooled naturally down to room temperature in the furnace to obtain C doped Ni$_3$S$_2$ NSs.

2. Electrochemical Characterizations

The electrocatalytic properties of the prepared samples were evaluated with Autolab (Aut72703) electrochemical workstation in a conventional three-electrode system. The C doped Ni$_3$S$_2$ NSs/Ni, Ni$_3$S$_2$ NSs/Ni were individually used as the working electrodes, a Hg/HgO electrode (1 M KOH, pH = 13.8) as the reference electrode, and a graphite plate as the counter electrode. The geometric surface area of the working electrode is 1.0×1.0 cm^2. The Hg/HgO reference electrode was calibrated with respect to RHE according to the previous study: in 1.0 M KOH, $E_{RHE} = E_{Hg/HgO} + 0.059pH + 0.098$. Prior to recording the electroactivity, the catalysts were activated by the continuous scans. Polarization curves were obtained using linear sweep voltammetry (LSV) in 1.0 M KOH with a scan rate of 1 mV s^{-1} and chronopotentiometric measurements were carried out under different overpotentials. The electrochemical impedance spectroscopy (EIS) was carried out at an overpotential of 100 mV in a frequency range from 100 kHz to 0.01 Hz. The polarization curves were corrected against ohmic potential drop.

3. Supporting Figures
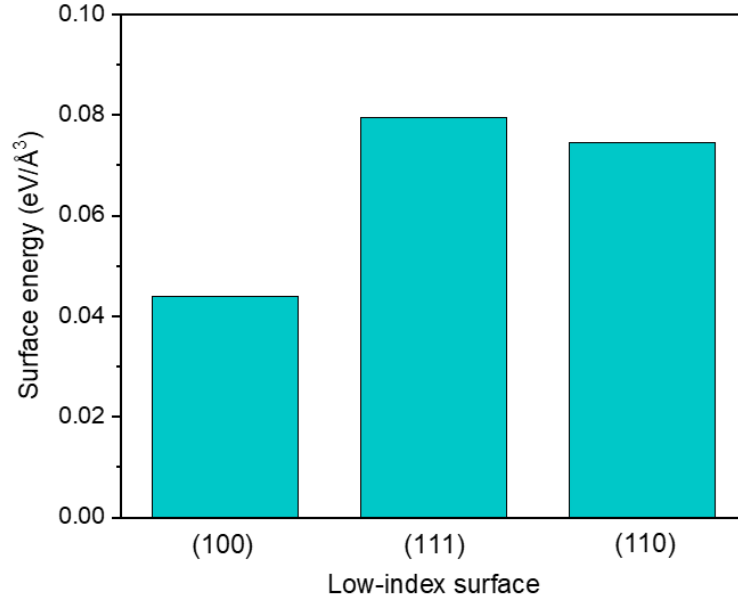
Figure S1. The surface energy (δ_S) of (100), (111) and (110) surfaces. (As the (001) and (010) have same structure as (100) and (101) has same structure as (110), we do not consider (001), (010) and (101) anymore. The δ_S is calculated according to $\delta_S = \frac{E_{(slab)} - N_{Ni}\mu_{Ni} - N_S\mu_S}{A}$, Where $E_{(slab)}$ is the energy of slab, N_{Ni}, N_S and N_X represent the number of Ni, S and X atoms respectively, and A is the surface area of a slab).
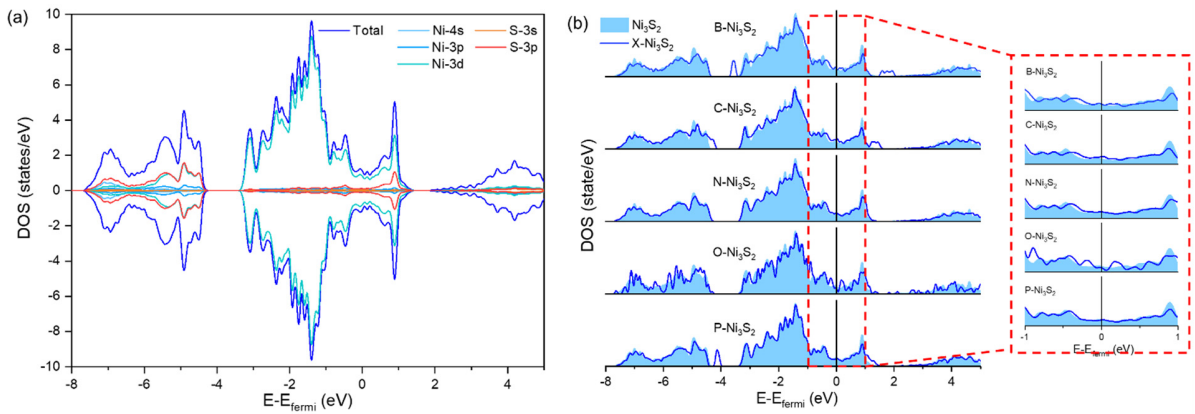

Figure S2. (a) The partial density of states for pure Ni_3S_2. (b) The total density of states for X doped Ni_3S_2 (only half of DOS is displayed).
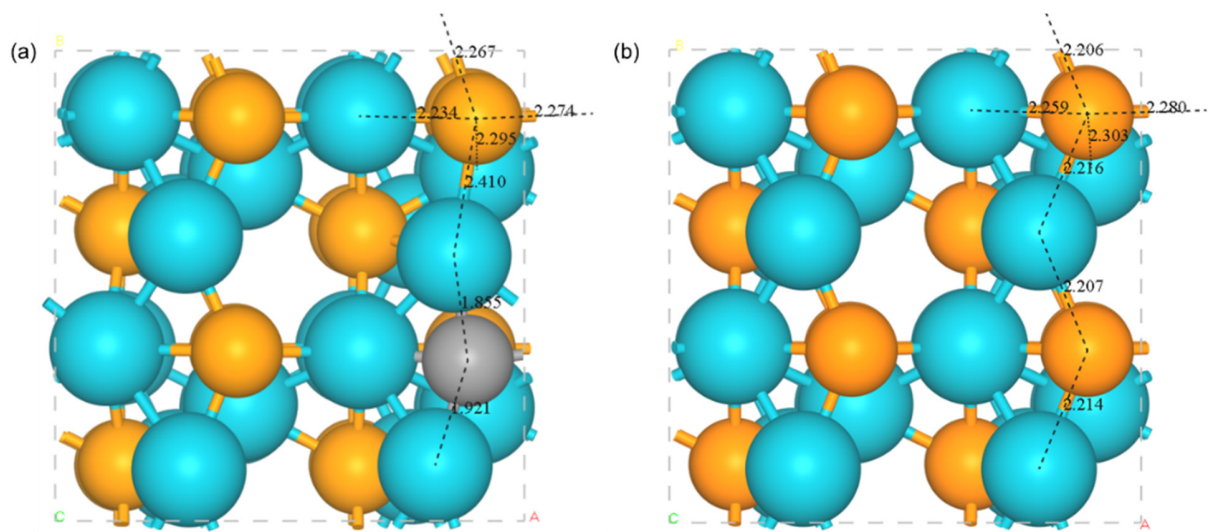
Figure S3. the Bond length of S3-Ni and X-Ni bonds on C_{out}-$Ni_3S_2(100)$ and $Ni_3S_2(100)$.
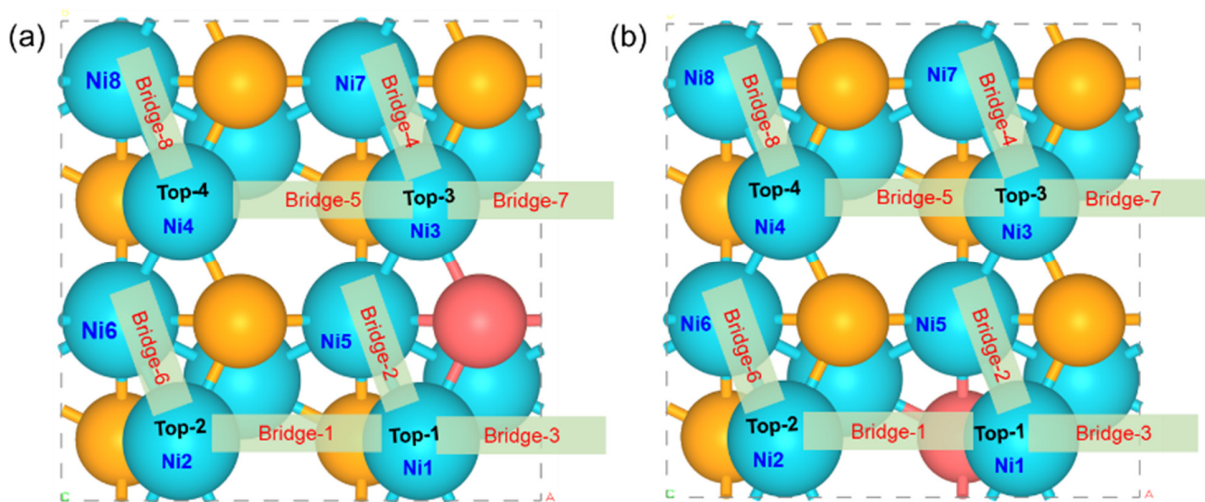
Figure S4. The adsorption site on (a) X_{out}-$Ni_3S_2(100)$ surface or pristine $Ni_3S_2(100)$ surface and (b) X_{in}-$Ni_3S_2(100)$ surface. (Top sites are for OH or OOH adsorption, while bridge sites are for O adsorption).
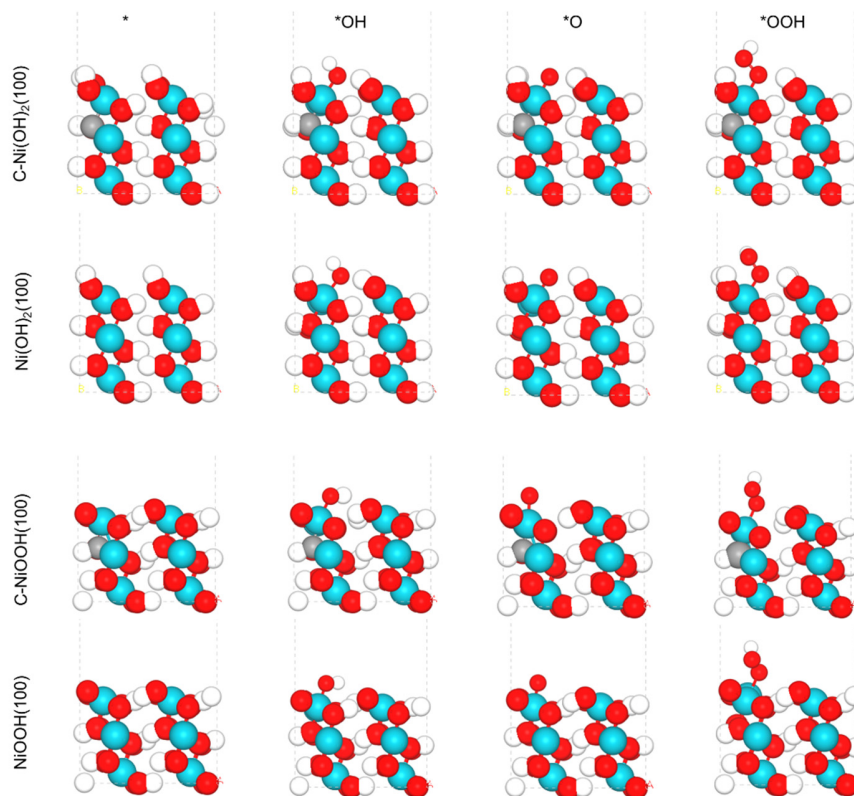
Figure S5. The structure of OER intermediats adsorption on prinstin and C doped Ni(OH)$_2$ and NiOOH.
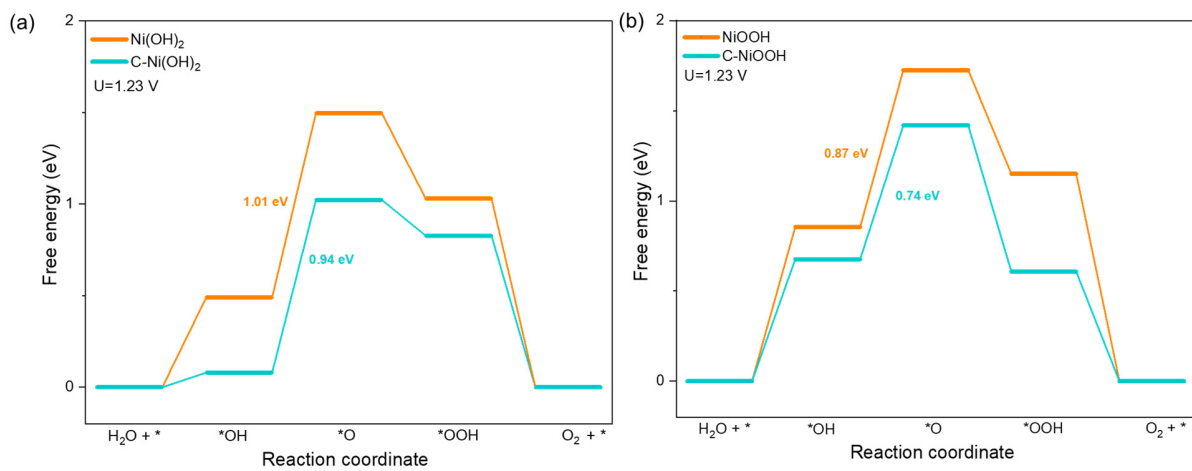
Figure S6. (a)-(b) Free energy diagram of OER on pristine and C doped Ni(OH)$_2$ and NiOOH respectively.
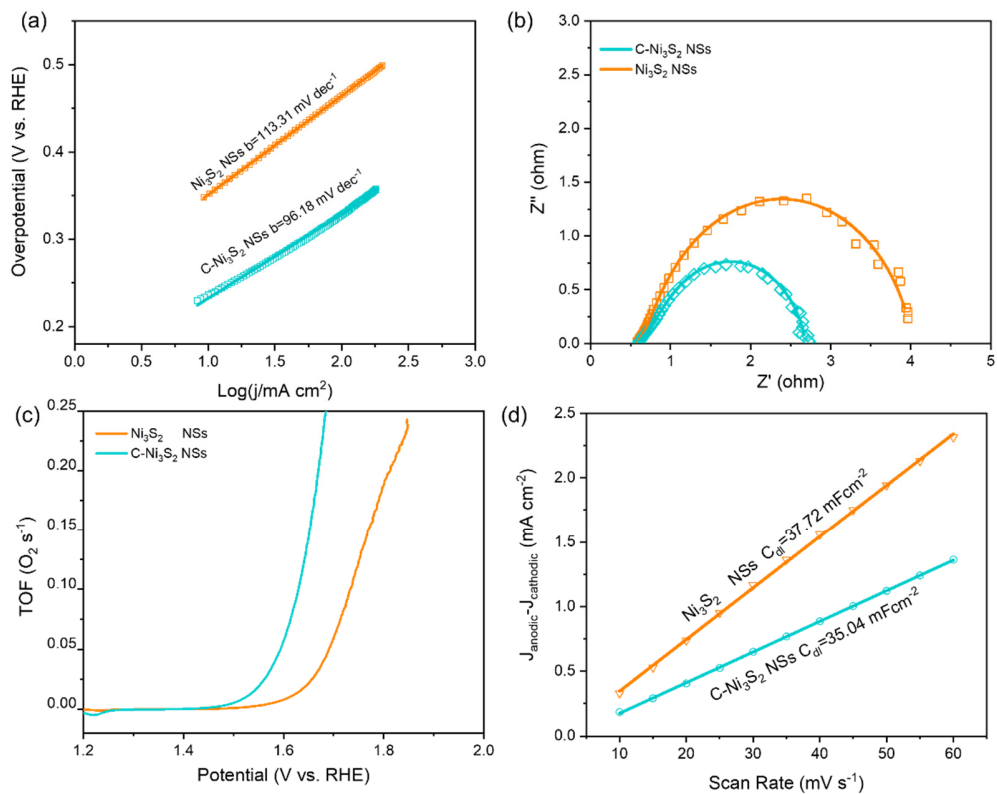
Figure S7. (a) The Tafel slop, (b) Nyquist plots obtained by electrochemical impedance spectroscopy. (c) turnover frequency (TOF) and (d) electrochemical double-layer capacitance of C- Ni_3S_2 NSs and Ni_3S_2 NSs.
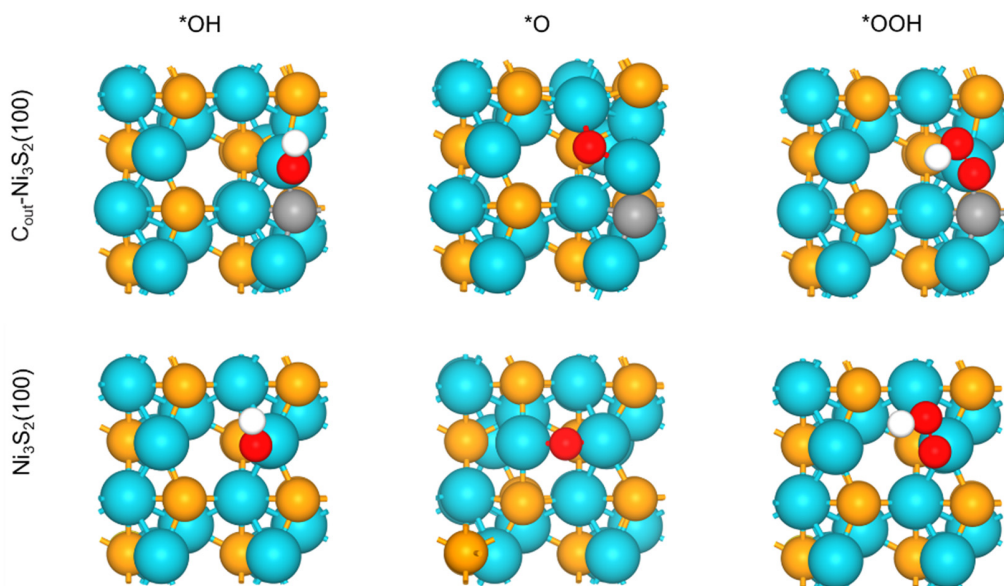
Figure S8. The structures of OER intermediates on Ni3 site of C_{out}-Ni_3S_2(100) and pristine Ni_3S_2(100).

4. Supporting Tables

Table S1. The bond length of X-Ni1 (d_{X-Ni1}) and Ni1-Ni5 ($d_{Ni1-Ni5}$) bonds, corresponding bonds length deviation after X doping (Δd_{X-Ni1} and $\Delta d_{Ni1-Ni5}$, more nagetive value means shorter bond), electronegativity (χ_x) and atom radius (R_x) of X.

| Distance	B_{out}-	C_{out}-	N_{out}-	O_{out}-	P_{out}-	B_{in}-	C_{in}-	N_{in}-	O_{in}-	P_{in}-
d_{X-Ni1} (Å)	2.045	1.921	1.921	2.044	2.209	2.017	1.911	1.891	1.965	2.238
Δd_{X-Ni1}(Å)	-0.169	-0.293	-0.293	-0.170	-0.005	-0.211	-0.317	-0.337	-0.263	0.010
$d_{Ni1-Ni5}$(Å)	2.531	2.492	2.493	2.541	2.552	2.487	2.490	2.427	2.493	2.561
$\Delta d_{Ni1-Ni5}$(Å)	-0.040	-0.079	-0.078	-0.030	-0.019	-0.084	-0.081	-0.144	-0.078	-0.010
$d_{Ni1-Ni2}$(Å)	4.253	4.284	4.252	4.156	4.107	3.937	3.755	3.738	3.831	4.075
$\Delta d_{Ni1-Ni2}$(Å)	0.170	0.201	0.169	0.073	0.024	-0.146	-0.328	-0.345	-0.252	-0.008
$d_{Ni3-Ni4}$(Å)	4.511	4.684	4.618	4.191	4.118	4.001	3.952	4.155	4.141	4.071
$\Delta d_{Ni3-Ni4}$(Å)	0.433	0.606	0.540	0.113	0.040	-0.077	-0.126	0.077	0.063	-0.007
d_{Ni1-S3}(Å)	2.232	2.267	2.265	2.244	2.206	2.178	2.204	2.232	2.203	2.198
Δd_{Ni1-S3}(Å)	0.026	0.061	0.059	0.038	0.000	-0.028	-0.002	0.026	-0.003	-0.008
d_{Ni5-S2}(Å)	2.339	2.364	2.344	2.247	2.288	2.220	2.235	2.286	2.310	2.264
Δd_{Ni5-S2}(Å)	0.059	0.084	0.064	-0.033	0.008	-0.060	-0.045	0.006	0.030	-0.016
$d_{Ni-S1/S5}$(Å)	2.229	2.289	2.279	2.219	2.234	2.220	2.232	2.328	2.270	2.214
$\Delta d_{Ni-S1/S5}$(Å)	0.001	0.061	0.051	-0.009	0.006	0.006	0.018	0.114	0.056	0.000
d_{Ni3-S3}(Å)	2.310	2.410	2.419	2.270	2.222	2.204	2.212	2.249	2.276	2.203
Δd_{Ni3-S3}(Å)	0.094	0.194	0.203	0.054	0.006	-0.012	-0.004	0.033	0.060	-0.013

Table S2. The adsorption free energy of OH, O and OOH on $Ni_3S_2(100)$ surface.

	Intermediates	Site	ΔG_{*ads} (eV)
	*OH	Ni1 top	**0.73**
		S_{out} top	1.92
	*O	Ni1 top	2.01
		Ni1-Ni2 bridge	**1.79**
		Ni1-Ni5 bridge	2.40
		Ni1-S_{out} bridge	1.97
	*OOH	Ni1 top	**3.74**
		S_{out} top	4.94
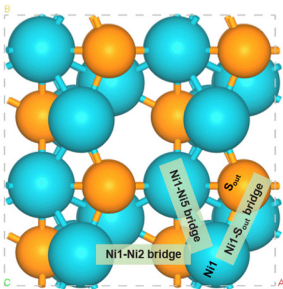
Table S3. The ΔG_{*OH} and ΔG_{*O} of C_{out}-$Ni_3S_2(100)$ and C_{in}-$Ni_3S_2(100)$ (as examples).

	ΔG_{*OH} (eV)			ΔG_{*O} (eV)	
ites	C_{out}-$Ni_3S_2(100)$	C_{in}-$Ni_3S_2(100)$	Sites	C_{out}-$Ni_3S_2(100)$	C_{in}-$Ni_3S_2(100)$
top-1	0.41	0.67	Bridge-1	1.57	1.97
			Bridge-2	2.19	1.74
top-2	0.67	1.04	Bridge-3	1.35	1.80
			Bridge-4	2.10	-
top-3	0.77	0.62	Bridge-5	-	1.81
			Bridge-6	-	2.55
top-4	0.78	0.76	Bridge-7	1.18	1.75
			Bridge-8	-	2.13

*Here, '-' means unstable O adsorption with O moved to another site.

Table S4. The comparison of OER activity between catalyst in this work and in recent works.

Catalysis	ŋ at 10 mA cm⁻² (mV)	Tafel slope (mV dec⁻¹)	Ref.
C-Ni_3S_2 NSs	261	95	This work
NiP/C	290	74	[1]
NiO/NC	420	61	[2]
Mn-Co_3O_4	332	60	[3]

NiFe LDH	290	51	[4]
P-Co$_3$O$_4$	280	52	[5]
P-Ni$_3$S$_2$	-	99	[6]
Co$_9$S$_8$ HMs	420	113	[7]
V-doped NiS$_2$	290	45	[8]
P-Co-Ni-S/NF	292	61	[9]
CuCo$_2$S$_4$ nanosheets	310	86	[10]

Table S5. Bader charge and b band center of Ni3 site and Ni site of C_{out}-Ni$_3$S$_2$(100) and Ni$_3$S$_2$(100)

Systems	Bader charge of Ni3 (e)	d band center of Ni3 (eV)
C_{out}-Ni$_3$S$_2$(100)	0.43	-2.07
Ni$_3$S$_2$(100)	0.39	-1.79

References:

[1]   Cheng, X.; Zheng, J.; Li, J.; Luo, X., Synthesis of Flower-Like Carbon-Doped Nickel Phosphides Electrocatalysts for Oxygen Evolution Reaction. *ChemistrySelect* **2019,** *4* (14), 4271-4277.

[2]   Seok, S.; Jang, D.; Kim, H.; Park, S., Production of NiO/N-doped carbon hybrid and its electrocatalytic performance for oxygen evolution reactions. *Carbon Letters* **2020,** *30* (5), 485-491.

[3]   Raj, S.; Anantharaj, S.; Kundu, S.; Roy, P., In situ Mn-doping-promoted conversion of Co (OH) 2 to Co3O4 as an active electrocatalyst for oxygen evolution reaction. *ACS Sustainable Chemistry & Engineering* **2019,** *7* (10), 9690-9698.

[4]   Zhong, H.; Liu, T.; Zhang, S.; Li, D.; Tang, P.; Alonso-Vante, N.; Feng, Y., Template-free synthesis of three-dimensional NiFe-LDH hollow microsphere with enhanced OER performance in alkaline media. *J. Energy Chem.* **2019,** *33*, 130-137.

[5]   Xiao, Z.; Wang, Y.; Huang, Y.-C.; Wei, Z.; Dong, C.-L.; Ma, J.; Shen, S.; Li, Y.; Wang, S., Filling the oxygen vacancies in Co 3 O 4 with phosphorus: an ultra-efficient electrocatalyst for overall water splitting. *Energy & Environmental Science* **2017,** *10* (12), 2563-2569.

[6]   Ding, Y.; Li, H.; Hou, Y., Phosphorus-doped nickel sulfides/nickel foam as electrode materials for electrocatalytic water splitting. *Int. J. Hydrogen Energy* **2018,** *43* (41), 19002-19009.

[7]   Zhang, Y.; Chao, S.; Wang, X.; Han, H.; Bai, Z.; Yang, L., Hierarchical Co9S8 hollow microspheres as multifunctional electrocatalysts for oxygen reduction, oxygen evolution and hydrogen evolution reactions. *Electrochim. Acta* **2017,** *246*, 380-390.

[8]   Liu, H.; He, Q.; Jiang, H.; Lin, Y.; Zhang, Y.; Habib, M.; Chen, S.; Song, L., Electronic structure reconfiguration toward pyrite NiS2 via engineered heteroatom defect boosting overall water splitting. *ACS nano* **2017,** *11* (11), 11574-11583.

[9]   Zhang, F.; Ge, Y.; Chu, H.; Dong, P.; Baines, R.; Pei, Y.; Ye, M.; Shen, J., Dual-functional starfish-like P-doped Co–Ni–S nanosheets supported on nickel foams with enhanced electrochemical performance and excellent stability for overall water splitting. *ACS applied materials & interfaces* **2018,** *10* (8), 7087-7095.

[10]   Chauhan, M.; Reddy, K. P.; Gopinath, C. S.; Deka, S., Copper cobalt sulfide nanosheets realizing a promising electrocatalytic oxygen evolution reaction. *ACS Catal.* **2017,** *7* (9), 5871-5879.